Sensors and Materials, Vol. 36, No. 6 (2024) 2337–2349
MYU Tokyo

S & M 3672

Development of Noncontact Microdistance-measurement Devices Based on Giant Magnetoresistance Sensors

Hung-Yih Tsai,[1] Ming-Chi Chiou,[1] and Ben-Fong Yu[2*]

[1]Department of Vehicle Engineering, National Formosa University,
No. 64, Wenhua Rd., Huwei Township, Yunlin Country 632301, Taiwan (R.O.C.)
[2]Graduate Institute of Precision Manufacturing, National Chin-Yi University of Technology,
No. 57, Sec. 2, Zhongshan Rd., Taiping Dist., Taichung City 411030, Taiwan (R.O.C.)

(Received January 3, 2024; accepted May 30, 2024)

Keywords: processing accuracy, noncontact microdistance sensor, GMR sensor, tool slider

Processing machines require various sensors for process monitoring and control to improve processing accuracy. Sensors become a critical factor in both automated production and intelligent manufacturing. It is interesting that the accuracy of the microdistance-measurement device affects the fine-tuning quality of cutting tools. In this work, we developed a noncontact microdistance sensor based on the giant magnetoresistance (GMR) effect by combining a neodymium magnet with a tool slider. The slider is displaceable along the axis of rotation adjustment. Thus, the distance between a neodymium magnet and GMR is altered when the rotary adjuster moves the tool slider. The corresponding voltage output can be measured under a changing magnetic field. The experimental results show that the measurement sensitivity can reach 4.68 mV/μm and that the linear output is approximately 2.54 V at the full-scale range. The significant advantage of being less prone to wear and not dampening the motion of a target of noncontact sensors leads to important applications in several areas of engineering and shows the potential for further improvement to provide a suitable structure for practical applications.

1. Introduction

Intelligent machine tools consist of measuring devices that monitor the real-time processing status through the Internet of Things.[1,2] The measuring devices are sensors for converting the detected physical quantity or phenomenon into an interpretable voltage or current signal. Since the magnetic field strength or direction changes due to strain, motion, rotation, or electric current can be measured without physical contact with the objects, magnetic sensors have been used in many industrial and navigation control systems. Magnetic sensors have been developed utilizing various physical phenomena such as the Hall Effect, electromagnetic induction, and giant magnetoresistance (GMR). There are many categories of magnetic sensors,[3] such as fluxgate magnetometers, magnetoinductive sensors, anisotropic magnetoresistive sensors, Hall sensors, GMR sensors, and magnetostrictive sensors. Among these magnetic sensors, the

*Corresponding author: e-mail: bfyu@ncut.edu.tw
https://doi.org/10.18494/SAM4874

ISSN 0914-4935 © MYU K.K.

resistance change in the magnetic field caused by GMR can be as high as 70%, indicating that the sensitivity of a GMR sensor is much higher than that of a Hall sensor. The applications of GMR to ammeter, differential ammeter, and power meter developments have been particularly fruitful.[4] The noncontact current measurement of the differential GMR sensor is isolated from the current source. It exhibits high anti-interference performance and sensitivity, with a sensitivity of up to 0.0307 V/A for sensing DC/AC current.[5] Commercial GMR-based sensors combined with a basic differential amplifier and an Arduino microcontroller detect GS-Fe_3O_4 magnetic nanoparticles and streptavidin in biosensor applications. The sensitivities to GS-Fe_3O_4 and streptavidin are 2.79 and 1.80 mV/(mg/mL), respectively.[6] For the detection of deflection, the GMR sensor can detect a displacement of 10 microlevels and its sensitivity can reach 0.0131 V/mm.[7] Furthermore, the application of GMR sensors in hybrid eddy current testing probes[8] shows that GMR sensors can significantly improve the measurement accuracy and range of eddy current testing. Therefore, GMR technology suits various processes such as current sensing, medical testing, and precision noncontact displacement measurement.

In this work, a microdistance-measurement device of a GMR-based sensor is used to measure the adjustment distance of a machine boring tool. In many boring tool fine-tuning devices, the rotation angle is proportional to the screw lead. Although a dial indicates the displacement when rotating a disk, the tool may not move because of backlash error. The design combines magnets with sliders, and a GMR sensor is used for noncontact measurement of the strength of the magnetic field to obtain the slider position, which can avoid the effect of backlash error and improve adjustment precision.

2. Device and Measurement Principle

The microdistance-measurement device involves fine-tuning structures and a measurement circuit. This device can be applied to boring tools and other applications that require microadjustment and measurement. Figure 1 shows a schematic of the microdistance-measurement device in which the round hole in the middle of the slider is used to install the tool. The magnet is embedded in the slider and moves with the rotation of the differential screw. Since the GMR sensor and the main circuit board are fixed to the body, the slider position can be directly measured without being affected by the clearance mechanism.

When the dial is rotated, both screws a and b rotate in the same direction; the number of rotations is N, resulting in leads p_a and p_b for screws a and b, respectively. According to the differential screw principle, the moving distance L of the sliding block along the axis of the rotating disk can be calculated as

$$L = N(p_a - p_b)\,. \tag{1}$$

Note that a decrease in rotation angle accompanies the decrease in the moving distance of the slider. The displacement dL of the slider relative to the change in the rotation angle $d\varphi$ can be obtained as

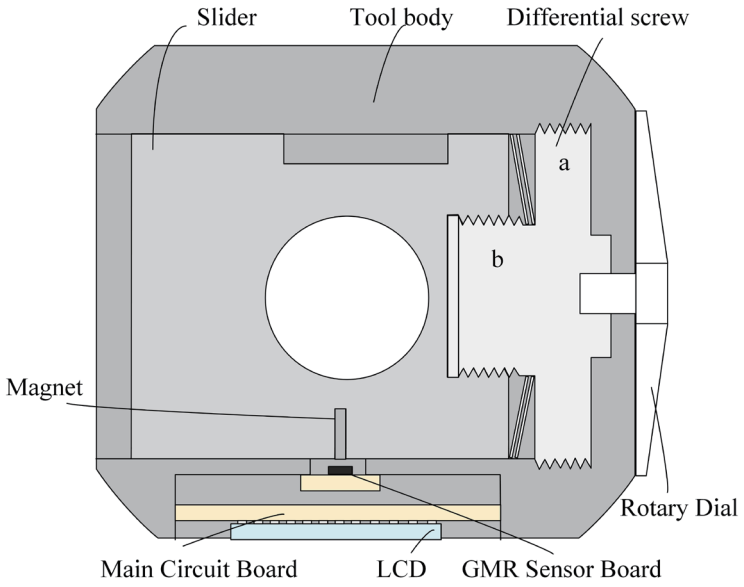

Fig. 1. (Color online) Schematic diagram of tool structure section.

$$dL = \frac{d\varphi}{2\pi}(p_a - p_b)\,. \tag{2}$$

In this study, we used the commercial GMR sensor ABL014 with a dual Wheatstone bridge structure. Figure 2 shows a schematic diagram of a single Wheatstone bridge, where *Vcc* supplies voltage and out1 and out2 form a differential output signal.

If the GMR sensor has a full-bridge architecture, $R1 = R2$ and $R3 = R4$. When the magnetic field changes, $R1 = R + \Delta R$; then, $R3 = R - \Delta R$. Therefore, the output voltage change can be expressed as

$$V_o = Vcc \times \frac{\Delta R}{R}\,, \tag{3}$$

where $\Delta R/R$ is the normalization of the resistance change ΔR of GMR by the most basic resistance R (resistance at zero magnetic field). The GMR sensing sensitivity is 0.04 %ΔR/Oe and is put into Eq. (2). When the magnetic field is smaller than the saturation magnetic field, the relationship between the magnetic field strength B and the output voltage can be obtained as

$$V_o = Vcc \times \frac{B \times 0.04\ \%}{R}\,. \tag{4}$$

The magnetic field strength at a distance d from the pole surface of the magnet is inversely proportional to the inverse square of the given distance,[5] which can be expressed as

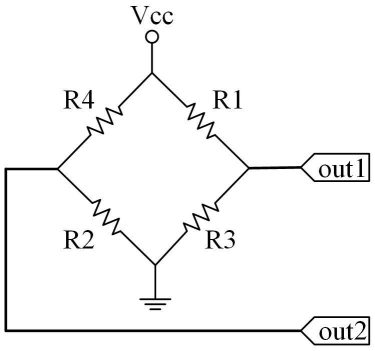

Fig. 2. GMR bridge.

$$B \propto \frac{1}{r^2}. \tag{5}$$

As shown in Fig. 3, $r = \sqrt{d^2 + x^2}$. The relationship between distance and magnetic field intensity can be expressed as

$$B = \frac{\mu \times H}{d^2 + x^2}, \tag{6}$$

where μ is the magnetic permeability ($u_0 = 4\pi \times 10^{-7}$ H/m is the vacuum magnetic permeability). Therefore, with the distance change dx, the change in magnetic field intensity can be expressed as

$$dB = \frac{\mu \times H}{d^2 + x^2} dx. \tag{7}$$

Through Eqs. (4) and (6), the sensed output voltage can be expressed as

$$V_o = \mu \times \frac{0.04\ \% \times Vcc \times H}{R \times \left(d^2 + x^2\right)}. \tag{8}$$

The change in output signal can be expressed as

$$dV_o = \mu \times \frac{0.04\ \% \times Vcc \times H}{R \times \left(d^2 + x^2\right)} dx. \tag{9}$$

When the signal amplifier has the gain g, the output voltage signal can be expressed by Eq. (10), and the voltage signal change can be expressed by Eq. (11).

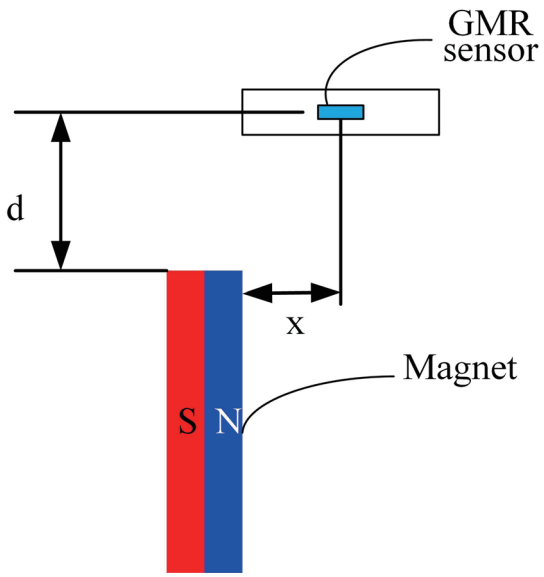

Fig. 3. (Color online) GMR and magnet position diagram.

$$V_o = g \times \mu \times \frac{0.04\ \% \times Vcc \times H}{R \times \left(d^2 + x^2\right)} \tag{10}$$

$$dV_o = \mu \times \frac{0.04\ \% \times Vcc \times H}{R \times \left(d^2 + x^2\right)} dx \tag{11}$$

Therefore, when the displacement of the slider is $dL = dx$, from Eq. (12), we determine that the relationship between the input and output of the system is

$$\frac{dV_o}{dL} = \frac{0.04\ \% \times \mu \times Vcc \times H}{R \times \left(d^2 + x^2\right)}. \tag{12}$$

It can be seen from the transfer function that, when the position changes, the change in output signal is directly proportional to the magnetic permeability, supply voltage, and magnetic field intensity. However, it is inversely proportional to the resistance and the square of the distance.

Figure 4 shows a diagram of the circuit architecture, which consists of a GMR sensor, an amplifier, a low-pass filter, a microcontroller, an LCD, and a temperature sensor. The output voltage from the GMR sensor is amplified by an instrumentation amplifier, and after RC low-pass filtering, it is captured by the analog-to-digital converter (ADC) of the microcontroller. The microcontroller calculates the distance and displays it on the LCD. The circuit has a digital temperature sensor and a reserved serial communication interface. It can be used for temperature compensation and other applications in the future.

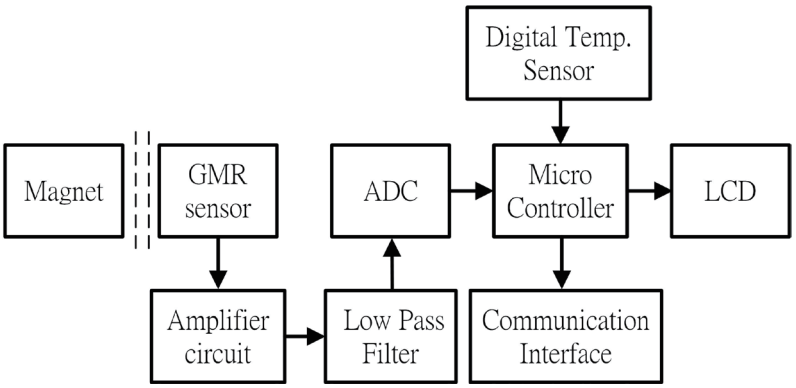

Fig. 4. Micromeasurement circuit structure diagram.

3. Experiment and Results

The measurement metric of the GMR sensor is the magnetic field strength. Therefore, it is necessary to know the relationship between the magnetic field strength and the gap of the magnet. The neodymium magnet used in this study is shown in Fig. 5. The size is 6.5 × 6.2 × 0.5 mm^3. A Gauss meter (F.W. BELL 5170) is used to measure the magnetic field strength of the neodymium magnet. Table 1 shows the average of the measured magnetic field strengths. The linear sensing specification range of ABL014 is ±100 Oe. Therefore, from the test values in Table 1, we determine that the distance between the magnet and the sensor is within 2.2 mm.

The microdistance-measurement circuit board prototype used in this study is divided into the main circuit board and the GMR sensor board. The two are connected using a flexible cable. Figure 6(a) shows a microcontroller on the main circuit board and devices such as an instrumentation amplifier, a low-pass filter circuit, and a power supply circuit, on the back. The size of the main circuit board is 35 × 30 × 7 mm^3. Figure 6(b) shows the GMR sensor board. In addition to the GMR sensor board, there is a voltage-stabilizing capacitor on the board. The size of the board is 9.5 × 6.5 × 3 mm^3. The arrow indicates the direction of movement of the sensed magnetic field.

Figure 7 shows the experimental mobile platform setup. A manual moving platform adjusts the gap between the GMR sensor and the magnet. The SIGMA KOKI TSDM60-20 moving platform moves the magnet laterally to generate displacement.

We used the laser displacement sensors Keyence LK-G5000 and LK-H008 to verify the displacement of the mobile platform. The accuracy of the laser displacement meter can reach 0.005 μm. As shown in Fig. 8, the linearity of movement of the mobile platform in short distances is good. Therefore, the benchmark quantity for subsequent tests was based on the displacement distance of the mobile platform.

The experimental architecture diagram is shown in Fig. 9. The test data acquisition uses the NI-DAQ USB-6343 data acquisition card. The experiment is divided into three parts. The first part is the GMR sensor output signal test. The second part is the signal processing test. The third

Fig. 5. (Color online) Neodymium magnet.

Table 1
Gap distance and magnetic field strength between the Gauss meter and the neodymium magnet.

Gap distance (mm)	Magnetic field strength (Gauss)
0	320.0
1.2	134.0
2.2	80.0
3.0	40.0

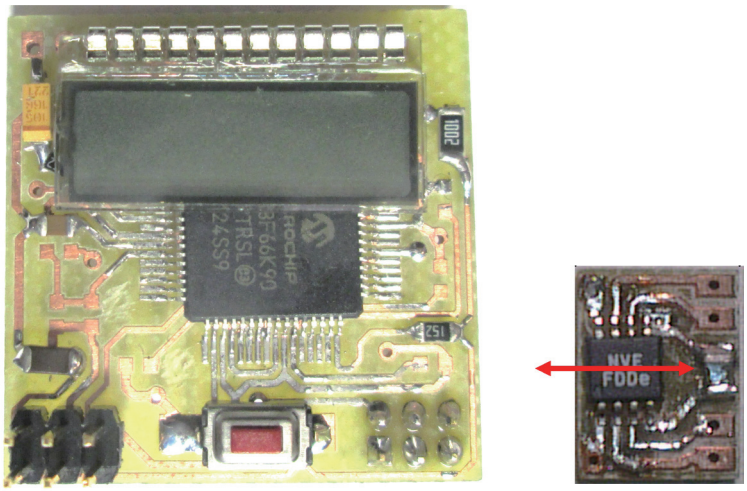

(a) (b)

Fig. 6. (Color online) (a) Main circuit board. (b) GMR sensor board.

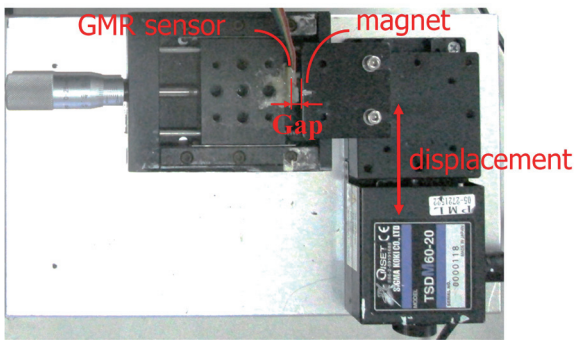

Fig. 7. (Color online) Displacement test platform.

part is the determination of error between the amount of movement calculated using the microcontroller through the characteristic equation and the position of the mobile platform.

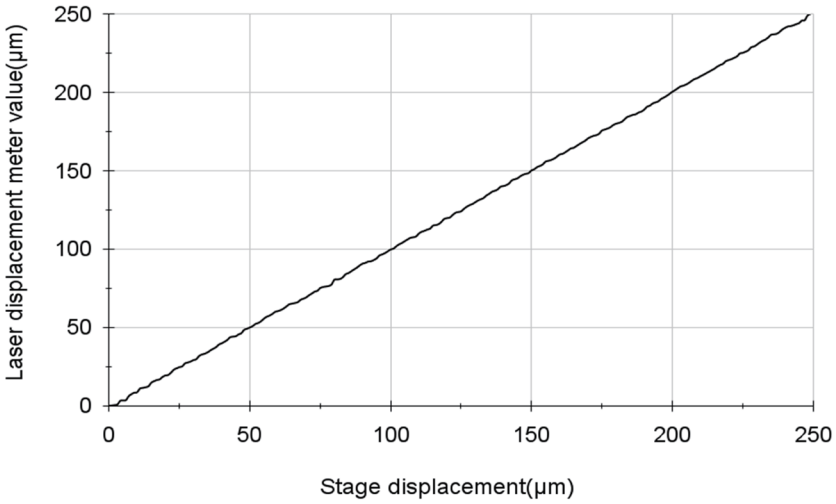

Fig. 8. Displacement platform test.

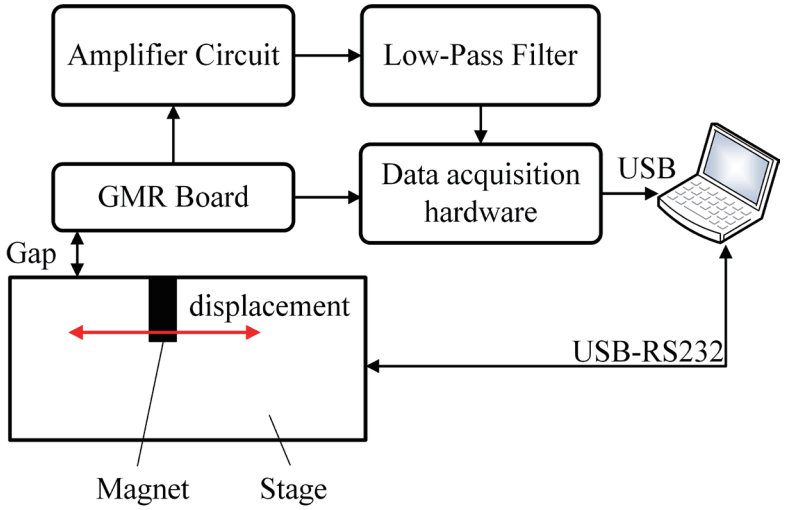

Fig. 9. (Color online) Schematic layout of the whole experimental setup.

First, we measured the GMR sensor output. GMR ABL014 has differential sensor elements that provide sinusoidal outputs and is a dual-bridge sensor producing sine and cosine waveforms at the output to give magnetic field strength information. The test was performed at gaps of 1.2, 2.2, and 3.0 mm. The displacement test outputs of the mobile platform are shown in Figs. 10–12. The distance between peaks is approximately 2.5 mm. The amount of change and linearity between the upper and lower peak voltages are needed in the microdistance measurement. The output curve with a gap of 1.2 mm exhibits the most significant change but has notable nonlinear changes. The gap range between 2.2 and 3.0 mm has better linear signals. Among them, the 2.2

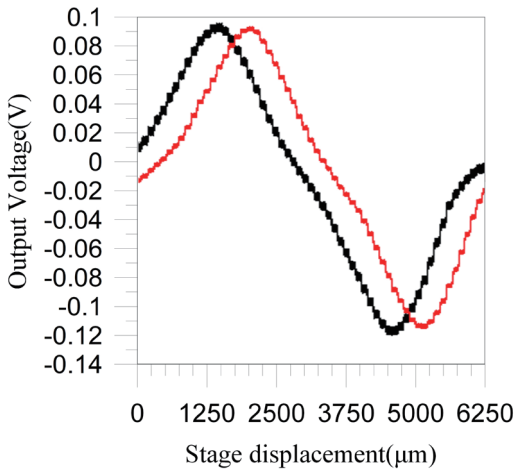

Fig. 10. (Color online) Output signal curve of 1.2 mm gap between magnet and GMR board.

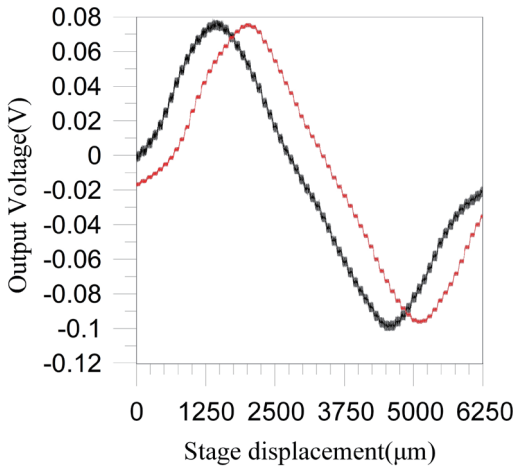

Fig. 11. (Color online) Output signal curve of 2 mm gap between magnet and GMR board.

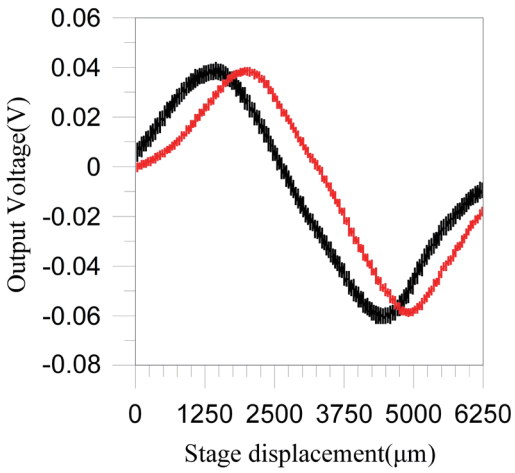

Fig. 12. (Color online) Output signal curve of 3 mm-gap between magnet and GMR board.

mm output signal sensitivity is higher. The magnetic field strength test results and GMR output show that the gap can still be fine-tuned. In subsequent experiments, the gap was slightly reduced to 2.0 mm to improve the measurement sensitivity without affecting linearity.

Since the ADC can only operate with a positive input voltage, microdistance measurement utilizes the positive voltage area. This means the displacement test is conducted in the N pole direction of the magnet. This design can also prevent nonlinear phenomena during N–S pole conversion. Because the movement distance of the fine-tuning device is 500 μm, the gain of the instrumentation amplifier is 50.4 times to improve the signal change. The cutoff frequency of the RC low-pass filter is 530 Hz.

Second, we used a mobile platform to conduct a 500-μm-displacement repeated test. The movement rate is 50 μm/s. In this experiment, the stage position where the output signal was 0.1

V was set as the origin point of the moving platform, which differs from the GMR output test. The output curve is shown in Fig. 13. The test 1 curve shows that the moving platform moves the magnet away from the sensor, and the test 2 curve shows that the magnet moves closer to the GMR sensor. The output curves are almost consistent and have good reproducibility.

We reduced the displacement speed for about 4 s to a displacement of 1 step (1 μm), captured the data, and observed the signal changes. The output voltage changes are shown in Fig. 14. The measured average voltage change for a displacement of 1 μm is about 5.08 mV. From the output characteristics shown in Fig. 13, it can be seen that the maximum voltage change in current applications is 0.1–2.64 V. When the microcontroller 12-bit ADC uses an external reference voltage of 3 V, the input resolution is approximately 0.732 mV/bit or 0.144 μm/bit.

Finally, the output characteristic curve shown in Fig. 13 was linearly fitted using a Google spreadsheet to obtain the following fourth-order equation:

$$l(v) = 1.19v^4 - 9.4185v^3 + 15.77v^2 + 198.9v - 23.15, \tag{13}$$

where l is the displacement and v is the output signal voltage after signal processing.

We used the microcontroller to calculate the displacement and subtracted the calculated displacement from the movement of the mobile platform to obtain the measurement error. Figure 15 shows the error curve. It can be seen that the change in error was concentrated at ±0.4 μm, and the maximum error was approximately ±0.65 μm, which meets the requirement of 1-μm-displacement measurement, which can adjust the low-pass-filter cutoff frequency or use a digital filter for higher stability to reduce the signal jitter and error. However, the response speed was reduced. It must be adjusted in accordance with the application response frequency requirements.

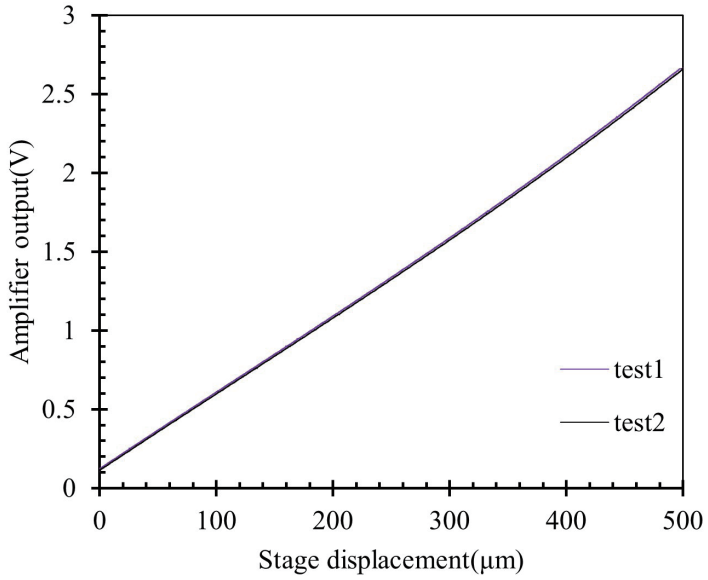

Fig. 13. Displacement output curve.

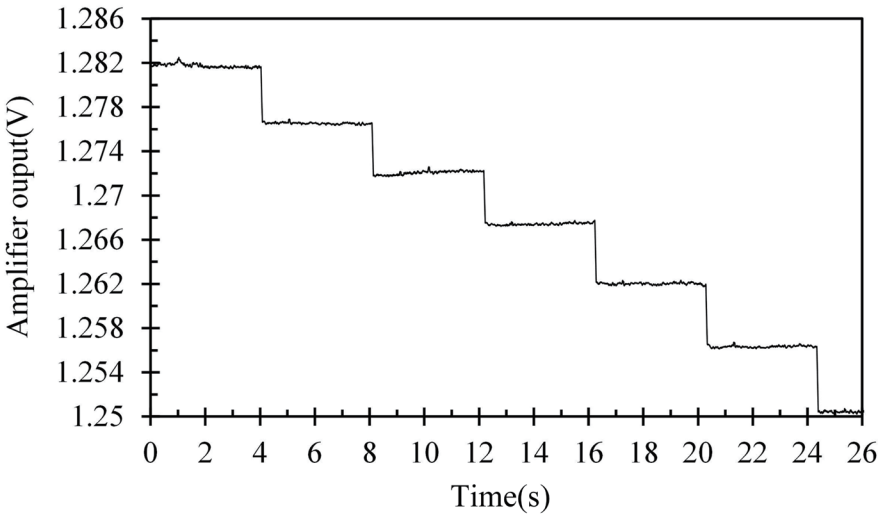

Fig. 14. Step test output signal.

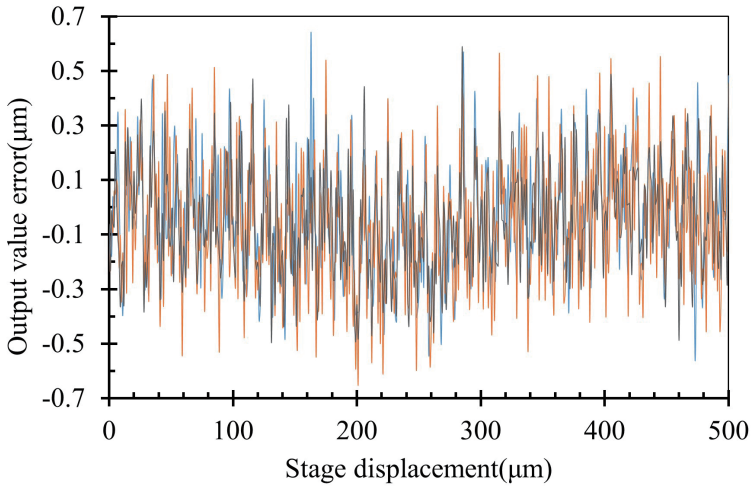

Fig. 15. (Color online) Measurement error.

4. Conclusions

In this study, we implemented a microdistance measurement device based on a commercial GMR sensor. At a gain of 50.4 of the instrument amplifier, the sensitivity reached 5.08 mV/μm. The linear output change was about 2.54 V. When the external reference voltage of the 12-bit ADC was set to 3 V, the resolution was about 0.144 μm/bit, which meets the measurement and calculation requirements. The displacement output error of the calculated output of the microdistance measurement device was approximately ±0.65 μm, which meets the measurement requirement of 1 μm. The round-trip curves almost overlap at a displacement rate of 50 μm/s. The hysteresis phenomenon is not apparent. The reproducibility of the displacement

measurement is good. In addition, the circuit structure is simple and easy to implement. It only requires a suitable magnetic field and a moving installation. It can be applied to other types of displacement measurement. We have proven the practicality of GMR measurement in fine-tuning the displacement of boring tools. This noncontact microdistance measurement using GMR-based sensors improves the processing precision of the adjustment distance. Therefore, the promising potential for further improvement makes this measurement system suitable for future practical applications.

Acknowledgments

We would like to acknowledge the financial support of the National Science and Technology Council, Taiwan, R.O.C., for this research under grant number NSTC 112-2221-E-150-036-.

References

1 T.-H. Liu, J.-Z. Chi, B.-L. Wu, Y.-S. Chen, C.-H. Huang, and Y.-S. Chu: Sensors **23** (2022) 1. https://doi.org/10.3390/s23010284
2 C.-W. Chang, H.-W. Lee, and C.-H. Liu: Inventions **3** (2018) 3. https://doi.org/10.3390/inventions3030041
3 M. J. Caruso, T. Bratland, C. H. Smith, and R. Schneider: Sensors-Peterborough **15** (1998) 34.
4 C. Reig, M.-D. Cubells-Beltrán, and D. R. Muñoz: Sensors **9** (2009) 7919. https://doi.org/10.3390/s91007919
5 C. Mușuroi, M. Oproiu, M. Volmer, and I. Firastrau: Sensors **20** (2020) 1. https://doi.org/10.3390/s20010323
6 H. Ardiyanti, N. A. Wibowo, N. I. Istiqomah, R. M. Tumbelaka, M. A. U. Absor, and E. Suharyadi: J. Sci.: Adv. Mater. Devices **8** (2023) 1. https://doi.org/10.1016/j.jsamd.2023.100556
7 A. Aminudin, R. D. Harnum, and M. Iryanti: J. Phys. Conf. Ser. **1280** (2019) 880. https://doi.org/10.1088/1742-6596/1280/2/022065
8 D. Rifai, A. N. Abdalla, K. Ali, and R. Razali: Sensors **16** (2016) 1. https://doi.org/10.3390/s16030298

About the Authors

Hung-Yih Tsai received his Ph.D. degree from National Chung Cheng University, Taiwan, in 2013. From 2013 to 2016, he was a postdoctoral researcher at National Chung Hsing University, Taiwan. From 2016 to 2019, he was a system integration assistant engineer and project leader at the Automotive Research & Testing Center. Since 2019, he has been an assistant professor at National Formosa University. His research interests are in mechatronics systems, vehicle electronics engineering, automation control, and sensors. (hungyih@nfu.edu.tw)

Ming-Chi Chiou received his Ph.D. degree from the University of Liverpool, United Kingdom. He is a professor at National Formosa University, Taiwan. He was the head of the Department of Vehicle Engineering from 1996 to 2022. His research interests are in mechanical heat flow, computational heat and mass transfer, and the experimental measurement of particle precipitation. (achi@gs.nfu.edu.tw)

Ben-Fong Yu received his B.S. degree from Da Yeh University, Taiwan, in 1999, his M.S. degree from National Chung Cheng University, Taiwan, in 2001, and his Ph.D. degree from National Chung Hsing University, Taiwan, in 2021. He worked for Goodway Machine Corp. and Ken Ichi Machine Co., Ltd., Taiwan, from 2002 to 2013 and from 2017 to 2021, respectively. Since 2022, he has been an assistant professor at National Chin-Yi University of Technology. His research interests are in mechanical design, vibration, thermal issues, mechatronics, and intelligent technology in machine tools. (bfyu@ncut.edu.tw)